Effects of solar radiation on convection and internal waves in ice-covered lake

Damien Bouffard[1], Roman E Zdorovennov[2], Galina E. Zdorovennova[2], Arkady Y. Terzhevik[2], and Alfred Wüest[1,3]

[1] Physics of Aquatic Systems Laboratory, Margaretha Kamprad Chair,
Ecole Polytechnique Federale de Lausanne, Switzerland
[2] Northern Water Problems Institute, Karelian Research Center,
Russian Academy of Sciences, Russia
[3] Surface Waters Research and Management, Eawag,
Swiss Federal Institute of Aquatic Science and Technology, Switzerland
damien.bouffard@epfl.ch

Abstract

Early-spring under-ice convection was investigated as part of an interdisciplinary research project in Lake Onego (Russia). We investigated temperature dynamics in the convectively-mixed and stratified layers of the lake with a thermistor chain and vertical profiling sensors. Radiative transfer through the ice led to a well developed convective mixed layer. Convective velocity was evaluated using two different methods and we showed that convective velocity is completely damped during the restratifying night time. We observed internal waves in the thermocline below the convective mixed layer with strong daily variations. Maximum of internal wave energy started in the afternoon and continued long after the end of solar radiation forcing. Our analysis indicates that local convective processes are key forcing mechanisms for the generation of internal waves in ice-covered lakes.

1 Introduction

Ice-covered lakes are protected from wind stress and exposed to only weak solar radiation (Farmer (1975)). In these extremely quiescent and low temperature environments (below 4°C), solar radiation can penetrate through ice and warms the underlying cold water. Mironov (2002) and Jonas et al. (2003) quantified the importance of radiatively-driven convection in ice-covered lakes.

Besides the importance of quantifying the under-ice convection as driver for early phytoplankton growth under ice, the role of the convection in the entire water column remains to be investigated. Of particular interest is the role of solar radiation in energizing the thermally inversely-stratified zone below the convectively-mixed layer (CML). Observations typically show internal wave activities in the winter thermocline that cannot be linked directly to wind forcing as is the case for open waters (Bouffard and Boegman (2012)). In ice-covered lakes, barotropic oscillations are generated by oscillations of the ice cover resulting from changes in atmospheric pressure and wind forcing (Bengtsson (1996)). Kirillin et al. (2009) observed baroclinic basin-scale internal waves (e.g. Poincare waves and Kelvin waves), and identified the forcing of these waves as a release of potential energy after lake freezing on the thermocline slope. Alternatively, laboratory and modelling activities have shown the potential for convective flow to initiate internal wave activities (Turner (1973)) through two different mechanisms. The first is associated with convective plume directly impinging the thermocline. Townsend (1964) used a tank with cold (below 4°C) stably-stratified freshwater heated from the top to demonstrate how convective

plumes generate internal waves as they imping onto the stable layer. Recently, Ansong and Sutherland (2010) showed that 4 % of the convective plume energy can be transferred to the internal wave field. The second is associated with nearshore density currents flowing along the slope before intruding the thermocline and generating progressive internal waves due to deflections caused by the fluid intrusion (Maxworthy et al. (2002); Flynn and Sutherland (2004); Nash and Moum (2005)).

2 Methods

2.1 Under-ice field measurements

Measurements were carried out in Lake Onego (Russia) in March 2015 at N61°48,744 / E34°25,793, in 27 m deep water. The under-ice measurements included a mooring (1 meteorological station, 3 pyranometers, 22 temperature loggers, 9 photosynthetically-active range (PAR) sensors) and round-the-clock vertical profiles (CTD and temperature microstructure profiler).

2.2 Scaling relations for convective mixing

We could not measure directly the convective velocity and used the scaling relation for convective turbulence described by Mironov et al. (2002):

$$w_c = (Bh_{cml})^{1/3} \tag{1}$$

with B ($\mathrm{m^2\ s^{-3}}$) the buoyancy flux in the convective layer spent to keep the convective layer vertically mixed and h_{cml}, the mixed layer thickness defined as the distance between the base of the diffusive under-ice layer (δ) and the bottom to the mixed layer (h_m), $h_{cml} = h_m - \delta$. The buoyancy flux was estimated using:

$$B = g\alpha_T(\delta)I(\delta) + g\alpha_T(h_m)I(h_m) - 2(h_m - \delta)^{-1}\int_{\delta}^{h_m} g\alpha_T(z)I(z)\mathrm{d}z \tag{2}$$

and, I ($\mathrm{K\ m\ s^{-1}}$) the kinematic radiation flux:

$$I(z) = \frac{E_d(z)}{\rho_0 C_p} \tag{3}$$

with, g, the acceleration of gravity, α_T the thermal expansion coefficient, ρ_0,a reference density of water, C_p the specific heat of water at constant pressure, and $E_d(z)$ the irradiance at a given depth. We also estimated the buoyancy flux in the shear-free convective layer by assuming steady state conditions in the turbulent kinetic energy (TKE) budget:

$$B = \frac{1}{c_2 h_{cml}}\int_{\delta}^{h_m} \epsilon(z)\mathrm{d}z \tag{4}$$

with c_2, a constant value term accounting for other terms preventing a one-to-one ratio between energy production by buoyancy flux and energy dissipation. Jonas et al. (2003) calculated a ratio of 0.74 between ϵ and B in the under-ice convective layer in Lake Vendyurskoe. The rate of dissipation ϵ of turbulent kinetic energy, was derived from

temperature microstructure measurements. From the convective velocity we estimated the convective energy, E_{conv}, (J m^{-2}) associated with the kinetic energy as:

$$E_{conv} = \frac{1}{2}\rho \int_{\delta}^{h_m} w_c^2 \mathrm{d}z \tag{5}$$

The rate of dissipation ϵ of turbulent kinetic energy was estimated using temperature fluctuation profiles measured by a Self Contained Autonomous Microstructure Profiler (SCAMP). We followed here the method used by Bouffard et al. (2012) and Bouffard and Boegman (2013), which consists in fitting the high frequency (100 Hz) temperature fluctuations to the Batchelor spectrum. We waited at least 20 min between two profiles to insure the artificial generated turbulence from the previous drop to be fully dissipated.

3 Results

3.1 Under-ice convection

The vertical structure of the water column under the ice is characterized by three layers (Fig. 1) during the penetrative convection phase: a thin under-ice gradient layer, a CML, and a stably stratified layer underneath. Fot the two weeks measurement period, the CML extended over 20 m. The convective velocity (Fig. 2a) estimated from the solar radiation (SR-based) method never exceeded 7.4 mm s^{-1}. The average maximum daily value was 3.9 mm s^{-1}. There is a very good agreement during daytime between the SR-based method (Eqs. 1, 2 and 3) and the dissipation-based method (Eqs. 1 and 4) An example of dissipation time serie is given on Fig. 2b and shows a strong decrease in ϵ in the CML at night. The dissipation-based method indicates a slow decay in the convective velocity (Fig. 2a) that cannot be seen from the first method based on solar radiation in which, by definition, the convective velocity is stopped at sunset. Nieuwstadt and Brost (1986) investigated the decay of convective turbulence by means of large eddy simulation in the case of a sudden drop of the forcing. They suggested that the decay time scales with the thickness of CBL and the upward convective velocity: $\frac{h_{cml}}{w_c}$. The parameterization of Nieuwstadt and Brost (1986) is in good agreement with the decay observed with the dissipation-based method and can be used to correct the SR-based method by including the decay of convective tubulence (not shown).

The thickness of the CML (20m) being much larger than the photic zone (5m), the first term in Eq. 1 is dominating and we can directly correlate the convective velocity to $I(\delta)$ (Fig. 2c). Although this simple parameterization does not reflect volumetric solar heating source, the best fit is given by $w_c = 6.8 \times 10^{-3} I(\delta) + 5.2 \times 10^{-9}$.

3.2 Internal waves

The stratified layer below the CML is prone to internal wave activity (Figs 1a, 1b). We observed a continuum of internal waves with periods from 50 s to 2 h with no preferential internal wave period excited (not shown). The most intriguing feature is the daily pattern of the short period ($<$ 2 h) internal wave activity (Fig. 1b). The isotherm displacements, as shown in Fig. 1b, indicated quiescent conditions in the morning followed by an increase in the wave amplitude of 0.6 m in the thermocline) in the afternoon until around midnight.

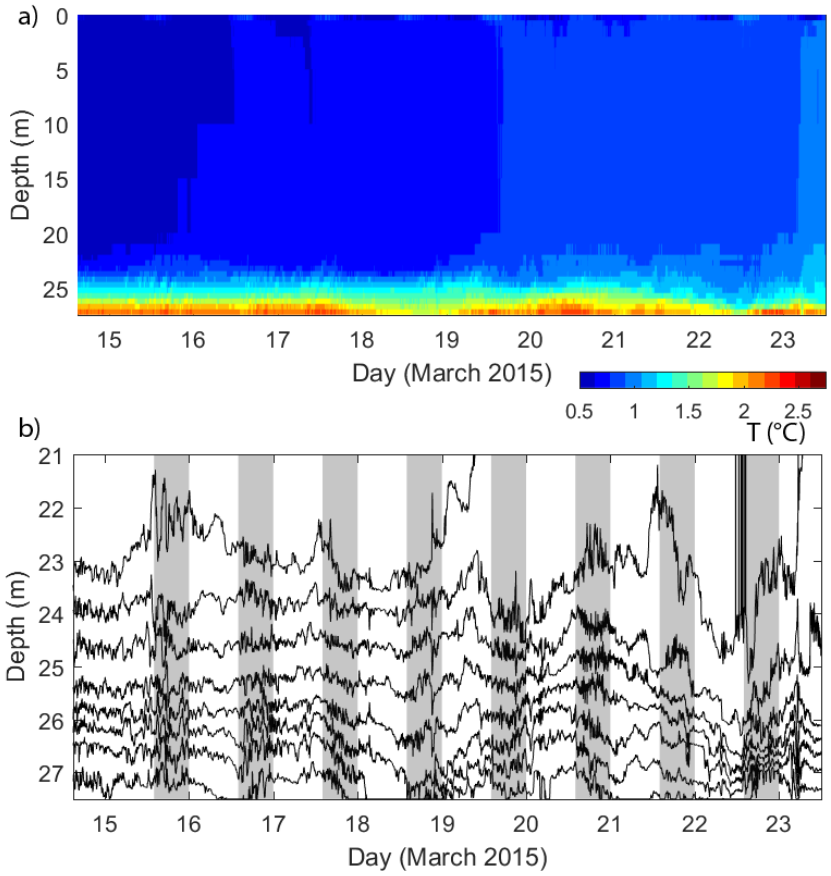

Figure 1: Contour plot of (a) temperature over the entire water column, and (b) isotherm displacement (0.2°C spacing). Shadded areaa highlight the increase in internal wave activity between 3pm and 12pm

4 Discussion and conclusion

The internal wave activity was analysed by calculating the internal wave energy, E_{IW}. E_{IW} is inferred from the available potential energy, APE, embedded in the band-pass filtered (300 s to 3600 s) wave-induced isotherm displacements (d_{IW}),$E_{IW} = 2APE$ (J m^{-2}), (Gill (1982)). E_{IW} is defined as:

$$E_{IW} = 2\frac{\rho}{2A_S}\int N^2(z,t)d_{IW}^2(z,t)A(z)\mathrm{d}z \tag{6}$$

With N (s^{-1}), the Brunt-Vasala frequency calculated from the thermistor chain, $A(z)$ and A_s (m^2) being the lake area at depth z and surface. Isotherm displacements extracted from the thermistor chain were band pass filtered (5 min to 1 h) to only represent the investigated internal wave oscillations.

The daily structure of the short period internal waves with weak oscillations in the morning and maximum oscillations from midday to midnight calls for the solar radiation as a trigger. The internal wave energy, E_{IW}, embedded in the range 5 min to 2 h is calculated using Eq. 6. The time series of normalized E_{IW} (Fig. 3) has a similar daily pattern to the oscillations of the normalized convective energy (Eq. 5, not shown) or the kinematic radiation flux, I (Fig. 3). However, we observed daily peaks in internal wave activity to occur between 6 pm and 10 pm or 8:30 pm on averaged, that is roughly 9 h after the peak in solar radiation occurs (Fig. 3).

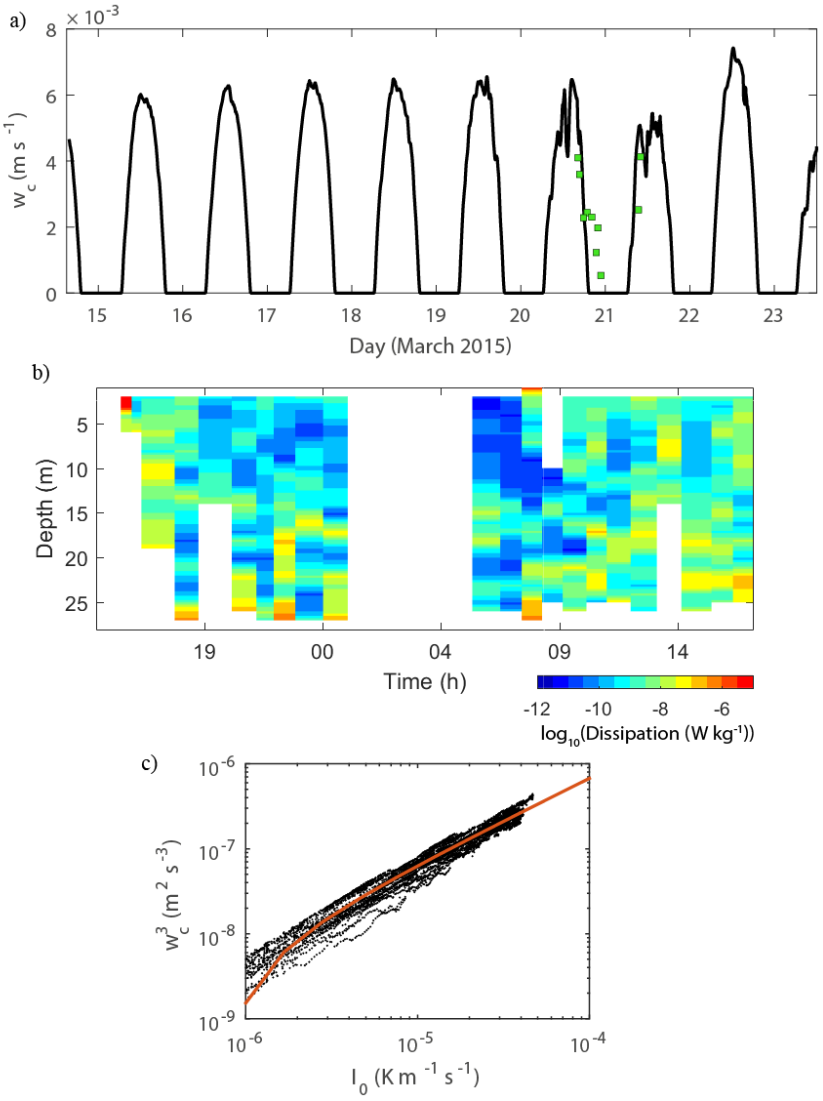

Figure 2: a) - Estimated convective velocity over the 10-days of observation using the SR-based method (line) and the dissipation-based method (square), b) dissipation measurements collected between March 21 and March 22; c) convective velocity as a function of the kinematic radiation flux at the upper limit of the convective layer. The red line represents the best fit.

Given this daily cycling, we tentatively linked the supply of E_{IW} to the solar radiation. We suggest two processes that may explain this energy supply: (i) Direct energy input from convective plumes impinging the thermocline (Ansong and Sutherland (2010)) or (ii): Remote energy input from shoreline excess heat flux leading to underflow (Kirillin et al. (2015)). The warmer water (denser) from sidearm may intrude into the thermocline and generate internal waves (Maxworthy et al. (2002); Flynn and Sutherland (2004); Nash and Moum (2005)).

We investigated (i) by considering E_{IW} as an integrator of the forcing I or E_{conv} (such as a capacitor integrates the electrical currents). From the temporal evolution of I and E_{IW} (Fig. 3), we show that E_{IW} is building up as long as the heat flux is positive and reaches therefore its maximum when the heat flux goes to zero. Similarly, the decay of E_{IW} stops as soon the thermal flux is starting in the morning (Fig. 3). We parameterized the time

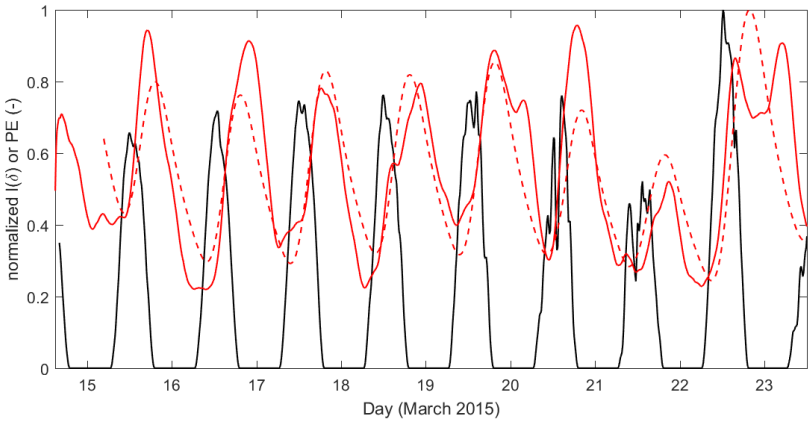

Figure 3: Time series of normalized kinematic radiation flux at $z = \delta$ (under the ice, in black) and internal wave energy (in red) Modelled internal wave energy based on kinematic radiation flux is shown in dashed red line. Max values set to 1.

evolution of E_{IW} as a function of $I(\delta)$ as $E_{IW}(t) = E_{IW}(t-1)e^{-\frac{\mathrm{d}t}{\tau_{IW}}} + a\int_{t-2\tau_{conv}}^{t} I(\delta)\mathrm{d}t$, with τ_{IW} the decay time scale of E_{IW} estimated from the data between 12pm and 6am, a, a constant fitting parameter, and τ_{conv} the decay time scale of the convective velocity as defined above. This simple parameterization is able to reproduce the daily variation of E_{IW} and the timing of energy peaks (Figure 3). Our results therefore suggest that the direct energy extraction from the convective plumes impinging the thermocline is a key source of under-ice internal wave generation.

The long-time shift (9 h) between E_{conv} (or $I(\delta)$ in Fig. 3) and E_{IW} peaks also points to a remote source of internal wave activity. Recently lateral heating has been shown as a source of density current in the early winter due to heat release from the sediments and in the late winter due to higher heating from ice melting in the shoreline and the catchment. Such density current typically generate internal waves when reaching the thermocline (Flynn and Sutherland (2004)) and could be a remote source of the observed oscillations. An analysis of the short-term internal wave properties (not shown) suggests a phase speed for short period internal waves of 0.06 m s^{-1}. While we didnt have any measurements to fully validate the hypothesis of density currents intruding the thermocline and generating internal waves, an estimate of the propagation time for the short period internal wave to travel the 2 km distance from the shore to the measurement site matches the 9 h averaged tiem delay betweent the solar peak and the internal wave peak. This process could also partly explain the time shift between the peak in SR and the observed peak in internal wave activity. We therefore suggest that (*ii*) hypothesis, i.e. nearshore density current driven by solar radiation, could also be responsible for energizing internal waves that propagate slowly offshore and for the peak in internal wave activities observed during the night. We encourage further experiments to fully investigate the potential role of density current generating internal waves in ice covered lakes.

References

Ansong, J. K. and Sutherland, B. R. (2010). Internal gravity waves generated by convective plumes. *Journal of Fluid Mechanics*, 648:405–434.

Bengtsson, L. (1996). Mixing in ice-covered lakes. *Hydrobiologia*, 322(1-3):91–97.

Bouffard, D. and Boegman, L. (2012). Basin Scale Internal waves. In *Encyclopedia of lakes and Reservoirs*, pages 102–107. Springer.

Bouffard, D. and Boegman, L. (2013). A diapycnal diffusivity model for stratified environmental flows. *Dynamics of Atmospheres and Oceans*, 61:14–34.

Bouffard, D., Boegman, L., and Rao, Y. R. (2012). Poincaré wave-induced mixing in a large lake. *Limnology and Oceanography*, 57(4):1201–1216.

Farmer, D. M. (1975). Penetrative convection in the absence of mean shear. *Quarterly Journal of the Royal Meteorological Society*, 101(430):869–891.

Flynn, M. R. and Sutherland, B. R. (2004). Intrusive gravity currents and internal gravity wave generation in stratified fluid. *Journal of Fluid Mechanics*, 514:355–383.

Gill, A. E. (1982). *Atmosphere-ocean dynamics*, volume 30. Academic press.

Jonas, T., Terzhevik, A., Mironov, D., and Wüest, A. (2003). Radiatively driven convection in an ice-covered lake investigated by using temperature microstructure technique. *Journal of Geophysical Research*, 108:3183.

Kirillin, G., Engelhardt, C., Golosov, S., and Hintze, T. (2009). Basin-scale internal waves in the bottom boundary layer of ice-covered Lake Mggelsee, Germany. *Aquatic Ecology*, 43(3):641–651.

Kirillin, G. B., Forrest, A. L., Graves, K. E., Fischer, A., Engelhardt, C., and Laval, B. E. (2015). Axisymmetric circulation driven by marginal heating in ice-covered lakes. *Geophysical Research Letters*, 42(8):2014GL062180.

Maxworthy, T., Leilich, J., Simpson, J. E., and Meiburg, E. H. (2002). The propagation of a gravity current into a linearly stratified fluid. *Journal of Fluid Mechanics*, 453:371–394.

Mironov, D. (2002). Radiatively driven convection in ice-covered lakes: Observations, scaling, and a mixed layer model. *Journal of Geophysical Research*, 107(C4).

Nash, J. D. and Moum, J. N. (2005). River plumes as a source of large-amplitude internal waves in the coastal ocean. *Nature*, 437(7057):400–403.

Nieuwstadt, F. T. M. and Brost, R. A. (1986). The decay of convective turbulence. *Journal of the Atmospheric Sciences*, 43(6):532–546.

Townsend, A. A. (1964). Natural convection in water over an ice surface. *Quarterly Journal of the Royal Meteorological Society*, 90(385):248–259.

Turner, J. (1973). Buoyancy effects in fluids. *Cambridge, University Press, 1973. 403 p.*